Condensation of DNA-actin polyelectrolyte mixtures driven by ions of different valences

Olena V. Zribi,[1] Hee Kyung,[1] Ramin Golestanian,[2,3] Tanniemola B. Liverpool,[2,4] and Gerard C. L. Wong[1]

[1]*Department of Materials Science & Engineering, Department of Physics, Department of Bioengineering,*
University of Illinois at Urbana-Champaign, Illinois 61801, USA
[2]*Isaac Newton Institute for Mathematical Sciences, Cambridge, CB3 0EH, United Kingdom*
[3]*Institute for Advanced Studies in Basic Sciences, Zanjan 45195-159, Iran*
[4]*Department of Applied Mathematics, University of Leeds, Leeds LS2 9JT, United Kingdom*

Multivalent ions can induce condensation of like-charged polyelectrolytes into compact states, a process that requires different ion valences for different polyelectrolyte species. In this work we examine the condensation behavior in binary anionic polyelectrolyte mixtures consisting of DNA coils and F-actin rods in the presence of monovalent, divalent, and trivalent ions. As expected, monovalent ions do not condense either component and divalent ions selectively condense F-actin rods out of the polyelectrolyte mixture. For trivalent ions, however, we observe a microphase separation between the two polyelectrolytes into coexisting finite-sized F-actin bundles and DNA toroids. Further, by increasing the DNA volume fraction in the mixture, condensed F-actin bundles can be completely destabilized, leading to only DNA condensation within the mixture. We examine a number of possible causes and propose a model based on polyelectrolyte competition for ions.

PACS number(s): 87.10.+e, 87.14.Gg, 64.75.+g, 61.25.Hq

I. INTRODUCTION

Electrostatics in complex fluids often exhibits counterintuitive effects [1–5]. In biology, one often encounters systems with strong electrostatic interactions (such as high surface charge densities and/or multivalent ions). Mean-field theories such as the Poisson-Boltzmann formalism, the usual starting point for understanding charged polyelectrolyte and colloidal systems, can no longer adequately describe the physics. In these cases, different forms of correlations between counter-ions can produce new interactions [6–10]. For example, like-charged attractions between polyelectrolytes may be possible due to the correlated fluctuations of the condensed ion layers around strongly charged polyelectrolytes [11–13]. A large number of recent theoretical investigations have focused on the existence and form of multivalent-ion-induced like-charge attraction between cylindrical polyelectrolytes [14–44] and on the collapse behavior of the polyelectrolyte itself [45–52]. Experimentally, counterion organization in the form of a charge density wave has recently been observed within F-actin bundles induced by divalent ions [53]. A number of excellent general reviews have also recently been published [3–5,54].

Like-charge attractions have been experimentally observed in a wide range of polyelectrolyte systems. It is also known that ions of different minimum valences are generally required to condense different polyelectrolytes. Trivalent ions are usually required to condense DNA, which is one of the most thoroughly studied systems in this context [55–69]. Recently, a number of rodlike anionic biopolymers (with persistence lengths of 1 μm or more) have been studied, such as the filamentous bacteriophages, microtubules, and F-actin [70,71]. Divalent ions are required to condense F-actin and viruses of the Ff family. In contrast to the above behavior for trivalent and divalent ions, monovalent ions do not condense any of these polyelectrolytes [9]. A number of interesting new effects have also been found. For example, in the pres-

ence of divalent ions, F-actin progressively condenses into close-packed bundles via an intermediate state comprised of liquid crystalline F-actin networks [52,72,73]. The dependence of DNA and F-actin condensation on ion valence, size, and structure has been systematically studied experimentally [66,70], and an empirically motivated criterion for the valence dependence has been proposed based on experimental results for "dumbbell" divalent ions [74].

Given that different polyelectrolytes are condensed by ions of different minimum valences, it is interesting to examine what happens when multivalent ions of a given valence are used to condense a mixture of two different polyelectrolytes with different condensation requirements. This represents a broad class of problems with many combinations. Individual polyelectrolyte parameters, such as charge density, contour length, and flexibility, can be varied, and the ion valence can be chosen to condense either or both of the polyelectrolytes in the mixture. The organization of the polyelectrolyte mixture can in principle have a wide range of structural possibilities, from ordered or disordered composite states to complete phase separation. The phase behavior of these mixed polyelectrolyte systems with multivalent ions has applications ranging from water purification to cystic fibrosis.

In this paper, we examine the ion-induced condensation behavior in binary anionic biological polyelectrolyte mixtures consisting of highly charged DNA coils and F-actin rods in the presence of monovalent ions (KCl, NaCl), divalent ions (CaCl$_2$, MgCl$_2$), and trivalent ions (spermidine chloride), using synchrotron small-angle x-ray scattering (SAXS) and laser-scanning confocal microscopy. As expected, monovalent ions do not condense either component and divalent ions selectively condense F-actin rods into bundles out of the DNA–F-actin polyelectrolyte mixture. Spermidine is a trivalent cation capable of condensing both polyelectrolyte species in isolation. We find that in the presence of spermidine, the system undergoes a microphase

separation into coexisting finite-sized, close-packed F-actin bundles and close-packed DNA toroids that can mutually adhere and assemble into large complexes, rather than collapse into a composite DNA–F-actin condensate. Further, by increasing the DNA volume fraction in the mixture, condensed F-actin bundles can be completely destabilized, leading to only DNA condensation within the mixture. It is clear that the presence of ions modifies the interaction between both similar and dissimilar polymer species (DNA-DNA, DNA-actin, actin-actin) within the mixture. Using this as a starting point, we consider a simple phenomenological Flory-Huggins theory for a mixture of polymers, rods, and the solvent and propose a model based on polyelectrolyte competition for ions.

II. MATERIALS AND METHODS

Lyophilized powder of rabbit skeletal muscle actin (G-actin, molecular weight =43 000) was purchased from Cytoskeleton (Denver). G-actin was suspended at 2 mg/ml in nonpolymerizing solution containing a 5 mM Tris buffer at pH 8.0, with 0.2 mM CaCl$_2$, 0.5 mM ATP, 0.2 mM DTT, and 0.01% NaN$_3$. Monovalent salt (KCl, final concentration 100 mM) was added to polymerize G-actin forming F-actin (diameter $D_{actin} \sim 7.5$ nm, charge density $\lambda_{actin} \sim -e/$ 0.25 nm at pH 7, persistence length $\xi_{actin} \sim 10$ μm). Samples were allowed to polymerize for 1 h at room temperature. The average length of F-actin filaments was controlled by adding human plasma gelsolin, an actin severing and binding protein, purchased from Cytoskeleton (Denver). (The F-actin average length dependence on gelsolin concentration has been previously calibrated [70].) To prevent F-actin depolymerization, actin was stabilized by addition of phalloidin (molecular weight =789.2; purchased from Sigma-Aldrich) at 1:1 molar ratio of phalloidin:G-actin. F-actin solutions were ultracentrifuged at 100 000g for 1 h to pellet the filaments. Supernatant buffer solution was then removed, and F-actin was resuspended in Millipore H$_2$O (18.2 MΩ) to the desired concentration. Lambda phage DNA (diameter D_{DNA} ~ 2.0 nm, charge density $\lambda_{DNA} \sim -e/0.17$ nm, persistence length $\xi_{DNA} \sim 50$ nm) was purchased from New England Biolabs, Inc. DNA was ethanol-precipitated and resuspended in de-ionized Millipore water (18 MΩ). Monovalent (KCl, NaCl) and divalent (CaCl$_2$, MgCl$_2$) salts (purchased from Sigma-Aldrich) are dissolved in de-ionized Millipore water (18 MΩ), and spermidine trihydrochloride (molecular weight 254.6; Sigma-Aldrich) is dissolved to generate trivalent ions (H$_3$N$^+$-CH$_2$-CH$_2$-CH$_2$-CH$_2$-N$^+$H$_2$-CH$_2$-CH$_2$-CH$_2$-N$^+$H$_3$) in solution. Mixtures of F-actin, λ-DNA, and salt solutions were combined, thoroughly mixed, and sealed in the quartz capillaries for x-ray studies. All experiments were performed at room temperature. Schematic representations of the polyelectrolytes and ions are given in Fig. 1.

For the confocal microscopy experiments, F-actin was dyed using Alexa Fluor 488 phalloidin (Molecular Probes) at a 1:1 monomer molar ratio and the DNA was dyed with POPO-3 (Molecular Probes) at a concentration of one dye molecule per 10 base pairs. Typical dilute sample concentrations were ~ 0.03 mg/ml for F-actin and ~ 0.02 mg/ml for
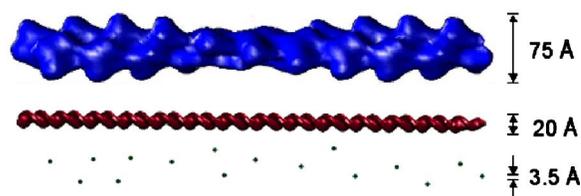
FIG. 1. (Color online) Schematic representation of solution components: F-actin rod (top, diameter $D \sim 75$ Å), DNA chain (middle, $D \sim 20$ Å), and salt ions (bottom, typical size ~ 3.5 Å). The length of DNA chains was fixed at 16 μm; the average F-actin length was varied between 0.3 and 10 μm.

DNA. To probe semidilute concentration regime, dyed F-actin and DNA were mixed with unlabeled F-actin and DNA in proportion of 1:100 labeled to unlabeled molecules. Typical semidilute sample concentrations were ~ 5 mg/ml for F-actin and ~ 1 mg/ml for DNA. The samples were imaged using a Leica TCS SP2 confocal microscope equipped with 63$\times$ oil immersion objective.

Small-angle x-ray scattering measurements were performed using both an in-house x-ray source as well as beamline 4-2 at the Stanford Synchrotron Radiation Laboratory (SSRL) and beamline 34-ID-C at the Advanced Photon Source (APS). For the in-house experiments, incident Cu $K\alpha$ radiation ($\lambda = 1.54$ Å) from a Rigaku rotating-anode generator was monochromatized and focused using Osmic confocal multilayer optics, and scattered radiation was collected on a Bruker 2D wire detector (pixel size =105 μm). For the SSRL BL-4-2 experiments, incident x rays were monochromatized to 10 keV ($\lambda = 1.24$ Å) using a double-bounce Si(111) crystal and focused using a cylindrical mirror with a beam size of 300×300 μm^2. The scattered radiation was collected using a MAR Research charged-coupled device camera (pixel size =79 μm). For the APS experiments, incident x rays were monochromatized to 9 keV ($\lambda = 1.38$ Å) using a double-bounce Si(111) reflection, with final beam size of 400 $\times 400$ μm^2. The scattered radiation was collected using a Roper Scientific direct-detection charge-coupled-device (CCD) camera (pixel size =20 μm). The two-dimensional (2D) SAXS data from all setups have been checked for mutual consistency. The 2D SAXS images were integrated using FIT2D software along two mutually perpendicular directions q_r and q_z, where q_r is along the equatorial direction and q_z is along the meridional direction (along the rod) [53].

III. RESULTS

To explore the ion-induced condensation behavior of a two-component polyelectrolyte mixture of F-actin and DNA, we used monovalent, divalent, and trivalent salts. (Our preliminary results show that ions of valence higher than 3 behave qualitatively the same way as trivalent ions in this context.) The condensation behavior of single-component polyelectrolyte solutions has been studied extensively [53,66,70,72,74–76]. The valence requirements for condensing DNA and F-actin are different. It was observed that monovalent salts do not induce condensation of either single-component solution, divalent salts induce condensation of
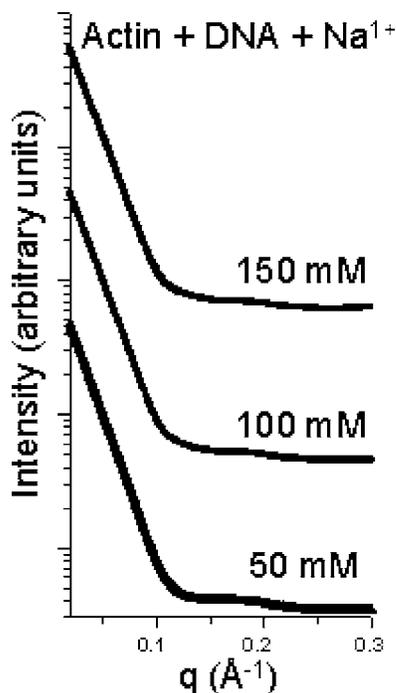
FIG. 2. Monovalent salt (NaCl) does not lead to condensation of either component in DNA–F-actin mixtures. The graph is a typical set of small-angle x-ray diffraction data for samples containing F-actin (average length 10 μm) at 5 mg/ml, λ-DNA at 1 mg/ml, and NaCl at 50–150 mM.

F-actin but not DNA, and trivalent salts can condense both. In the following sections, the condensation behavior of binary polyelectrolyte mixtures of F-actin and DNA has been examined in the presence of different monovalent (K, Na), divalent (Ca, Mg), and trivalent (spermidine) ions. Specifically, we want to investigate how F-actin–DNA interactions affect the condensation of each component. In principle it is a system with a wide range of possibilities. For example, the presence of one polyelectrolyte may affect the condensation behavior of the other or the mixture may cocondense into a composite state.

A. Monovalent salt

λ-DNA at the concentration range of 1–5 mg/ml is organized as an isotropic phase of flexible coils. In contrast, F-actin at 5 mg/ml can be either isotropic or nematic, depending on the F-actin length and the ambient salt conditions [77–79]. Mixtures of isotropic DNA and nematic F-actin can in principle phase separate. Phase separation between DNA and F-actin has been observed in mixtures with no added salt [80]. We have done experiments to assess how this arrangement is modified in the presence of monovalent salt. X-ray diffraction studies show that monovalent salts (KCl, NaCl) do not induce either F-actin or DNA condensation in two-component mixtures (Fig. 2). We examined F-actin+DNA +NaCl mixtures using x-ray diffraction. The diffraction pattern has been integrated along a 30° wedge along q_r. As shown in Fig. 2, the structure factor along q_r is featureless and shows a smooth monotonic decrease. No correlation

peaks were observed over a wide range of monovalent salt concentrations (0–150 mM). This result does not depend on the type of monovalent cation used. Similar results have been obtained for F-actin+DNA+KCl, so this is not an ion-specific effect. We conclude that the behavior of F-actin–DNA mixtures is similar to the behavior of the corresponding one-component polyelectrolyte+monovalent salt systems. In these single-component polyelectrolyte systems, monovalent counterions can only screen the electrostatic repulsions, but cannot generate attractions [3,4,74].

B. Divalent salt

One-component F-actin+divalent salt mixtures have been previously shown to exhibit a number of condensed phases [72]. For example, at low ion concentrations (0–3 mM), no condensation is seen. As expected, depending on the global concentration of F-actin, either an isotropic phase or a nematic phase can be observed. At high divalent ion concentrations (25–90 mM), condensed F-actin bundles are observed, with a first-order peak at 0.086 Å^{-1}, which indicates close packing of the individual filaments [53]. At intermediate divalent ion concentrations (3–15 mM), however, a liquid-crystalline network phase is observed [72], which consists of F-actin filaments cross-linked by divalent ions. This network phase of actin comprises layers of actin filaments. The actin filaments are oriented transverse to the layering direction, with liquidlike correlations within each layer. These layers are in turn cross-linked by ions into smecticlike stacks. The network is organized at larger length scales than the close-packed bundles, with diffraction features observed at 0.035 and 0.067 Å^{-1}, the intensities of which depend on average F-actin length. In the concentration range of 15–25 mM the liquid-crystalline network phase and bundled phase coexist. It can be shown that these phase domain boundaries depend on the F-actin rod lengths. In contrast, most divalent salts are incapable of inducing DNA condensation [57,63,74].

In Fig. 3, we examine two-component F-actin+DNA +Mg polyelectrolyte mixtures. The diffraction pattern has been integrated along a 30° wedge along q_r. At low divalent salt levels (<3 mM) we find no correlation peaks that indicate a condensed phase for either component. At intermediate salt concentrations (~5–20 mM) we find diffraction peaks at 0.035 and 0.067 Å^{-1}. The positions of these peaks are consistent with the previously observed diffraction signature for the liquid-crystalline network phase of F-actin [72]. At high divalent salt levels we observe diffraction maxima at 0.086 Å^{-1} and 0.136 Å^{-1} that are indicative of a bundled phase of F-actin rods [53]. From these results, we can see that the sequence of condensed F-actin phases is preserved in the presence of DNA. We observe no additional diffraction maxima that could be attributed to DNA condensation in the entire range of salt concentrations examined. In other words, the presence of condensed F-actin does not enhance DNA condensation in F-actin–DNA mixtures with divalent ions, and likewise, the presence of DNA in a solution of F-actin and divalent salt does not prevent F-actin condensation.

C. Trivalent salt

Trivalent ions can be used to condense both DNA and F-actin in single-component polyelectrolyte solutions. It
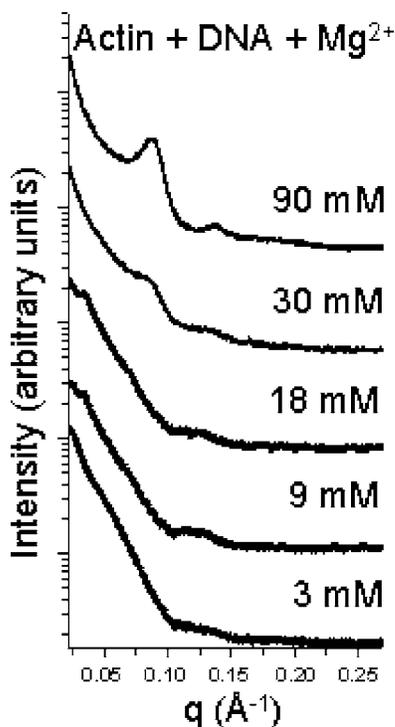
FIG. 3. Divalent salt ($MgCl_2$) will condense F-actin preferentially out of DNA–F-actin mixtures. A typical set of small-angle x-ray diffraction data for samples containing F-actin (average length ~ 1 μm at a concentration of 5 mg/ml) and λ-DNA (16 μm, 2.28 mg/ml) for $MgCl_2$ concentrations from 3 mM to 90 mM is shown. Progressive condensation of F-actin is observed at increasing salt concentration. Diffraction peaks at 0.035 and 0.067 Å^{-1} correspond to the first and second harmonics of the condensed lamellar network phase of F-actin at 5–20 mM salt [72]. These peaks are generally weak for long F-actin and strong for short F-actin. The diffraction feature at 0.086 Å^{-1} at 30–80 mM salt corresponds to the close-packed bundled phase of F-actin. DNA condensation peaks are not observed.

has been previously shown that DNA can be condensed upon addition of sufficient amount of trivalent salt [17,57,63,66,75,76]. The same is true for F-actin [71]. A bundled phase of F-actin (at 5 mg/ml) can be induced by addition of spermidine[3+] at concentrations above ~ 1.5 mM. This can be seen in Fig. 4. Correlation peaks can be observed at 0.086 and 0.136 Å^{-1}, which corresponds to a condensed phase with an interactin distance of ~ 75 Å. This is essentially the same close-packed structure observed for pure F-actin condensed with divalent ions. If both DNA and F-actin were combined together with trivalent salts such as spermidine, the resulting condensates can in principle have a number of possible structures. For example, it would be geometrically possible to intercalate DNA chains in the interstices of a close-packed columnar hexagonal F-actin lattice. To investigate the large-scale organization of F-actin–DNA condensates we investigated fluorescently labeled dilute (~ 0.01 mg/ml for both F-actin and DNA concentrations) and semidilute (~ 1 mg/ml for both F-actin and DNA concentrations) F-actin–DNA mixtures using confocal microscopy. In both concentration regimes we observe that the
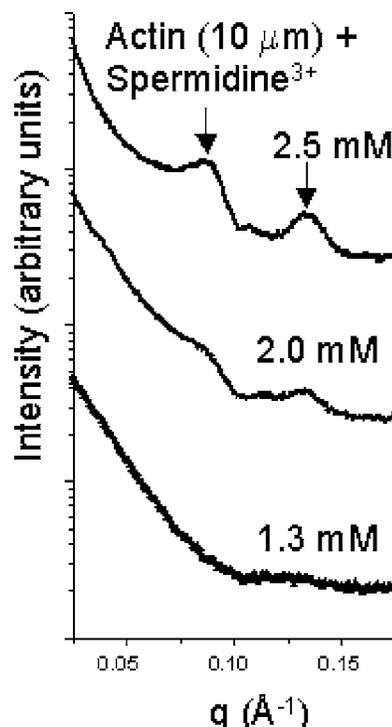
FIG. 4. Condensation of F-actin by spermidine[3+] in the absence of DNA: typical sets of SAXS data for samples containing F-actin (average length 10 μm) at 5 mg/ml and spermidine[3+] from 1.3 mM to 2.5 mM are shown. Diffraction peaks from the condensed bundle phase at 0.086 Å^{-1} and 0.136 Å^{-1} can be observed at high spermidine concentrations. The onset of condensation is above ~ 1.5 mM spermidine.

F-actin–DNA system undergoes a microphase separation into coexisting pure F-actin condensates (green) and pure DNA condensates (red). The F-actin condensates usually take the form of finite-sized bundles. In contrast, the DNA condensates usually take the form of finite-sized globules. For these low-concentration samples, it is likely that these globules correspond to generic toroidal structures observed for condensed DNA, details of which cannot be resolved by optical microscopy [Fig. 5(a)]. These bundles and globules have typical sizes that range from the submicron to micron range [75] (microscope point spread function ~ 0.25 μm). Moreover, these objects can mutually adhere to one another and assemble into composite aggregates consisting of large numbers of F-actin bundles and DNA globules [Fig. 5(b)]. At higher F-actin and DNA concentrations (1–5 mg/ml, semidilute regime), we observe heterogeneous aggregates consisting of F-actin bundles and more complex geometries of DNA condensates, including DNA bundles [Figs. 5(c) and 5(d)]. These finite-sized DNA bundles may be due to the coalescence of DNA globules [Fig. 5(c) and 5(d)], and their existence is consistent with observations of Iwataki *et al.* for pure DNA+spermidine mixtures [75]. Further, it can be seen that the local concentration of condensed DNA globules is significantly enhanced in the proximity of F-actin bundles, consistent with the above observation of mutual adhesion between DNA and F-actin condensates. Attractive interactions such as van der Waals attractions and electrostatic cor-
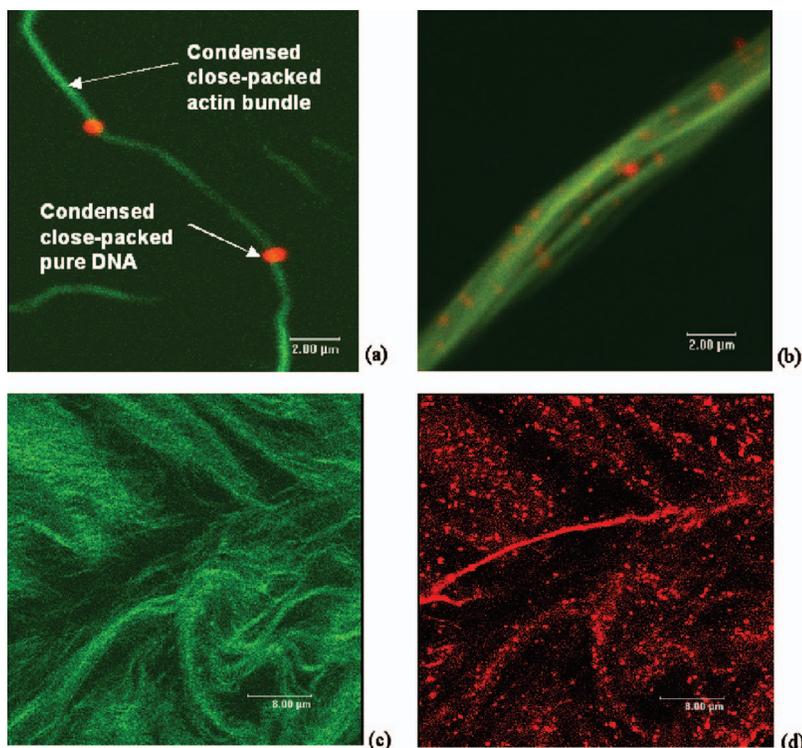
FIG. 5. (Color) Structure of F-actin–DNA–spermidine^{3+} condensates from confocal microscopy: F-actin (10 μm average length) was dyed with Alexa Fluor 488 (green); λ-DNA (16 μm length) was dyed with POPO-3 (red). (a) Close-packed DNA globules (presumably toroids) adhere to close-packed F-actin bundles. These structures can in turn organize into larger composite bundles (b). The spermidine^{3+} concentration is 10 mM, which is sufficiently high to condense both species. The molar ratio between DNA base pairs and monomeric G-actin is $D/A=15$. Global concentration of F-actin is 0.03 mg/ml, DNA 0.023 mg/ml. (c),(d) At high polyelectrolyte concentrations (actin 5 mg/ml, DNA 1 mg/ml) and high salt levels (spermidine^{3+} 5 mM) large aggregates of F-actin bundles and more complex geometries of DNA condensates are observed. Panels (c) and (d) represent same spot in the sample where exposures for F-actin (c) and DNA (d) are separated for clarity.

relations in strongly bound spermidine ions between the toroids and bundles can potentially contribute to this composite F-actin–DNA organization. In the context of the current debate on the physical origin of observed condensed polyelectrolyte bundle sizes [21,81–83], it is interesting to note that F-actin bundles preferentially adhere to DNA globules or weakly aggregate into a nematic network with other F-actin bundles rather than form close-packed bundles of larger radii from individual actin filaments. Moreover, we do not observe the evolution of these aggregates into larger radii bundles (within the experimental duration of $\sim$24 h). These observations suggest a thermodynamic limit to the bundle size, although more work will be necessary in order to elucidate the interactions between the DNA and F-actin condensates. For example, it is possible that DNA toroids preferentially adhere to bundles rather than to other toroids due to the reduced surface curvature. It is clear from these experiments, however, that the DNA and F-actin do not pack together into a homogeneous composite structure within these condensates.

The microscopic organization of these DNA–F-actin condensates can be seen in a series of synchrotron SAXS experiments [Figs. 6(a) and 6(b)] for samples at different DNA base pairs to actin monomer(G-actin) molar ratios (D/A). The DNA concentration was varied between 1.14 and 3.8 mg/ml for constant F-actin and spermidine^{3+} concentrations (5 mg/ml and 5 mM, respectively). This corresponds to 0.12 mM concentration of actin monomers and 1.7–5.8 mM concentration of DNA base pairs. Figure 6(a) shows a sample at $D/A=30$. Two sets of diffraction peaks can be observed, corresponding to F-actin correlations within the bundles (single arrow, interactin spacing =73 Å) and DNA correlations in the globules and bundles (double arrow, inter-DNA spaacing =25 Å), which indicates near close packing of the filaments. We observe one diffraction peak

from condensed DNA, so it is not possible to assign a unique surface unit cell to it. However, the position of the peak suggests that the DNA is close packed or very nearly so. If we assume that the DNA were organized into a hexagonal lattice, then this observed peak would correspond to the q_{10} diffraction for a columnar lattice, with a lattice parameter of $a=4\pi/(\sqrt{3}q_{10})$. The data indicate $q_{10}=0.245$ Å^{-1}; this corre-
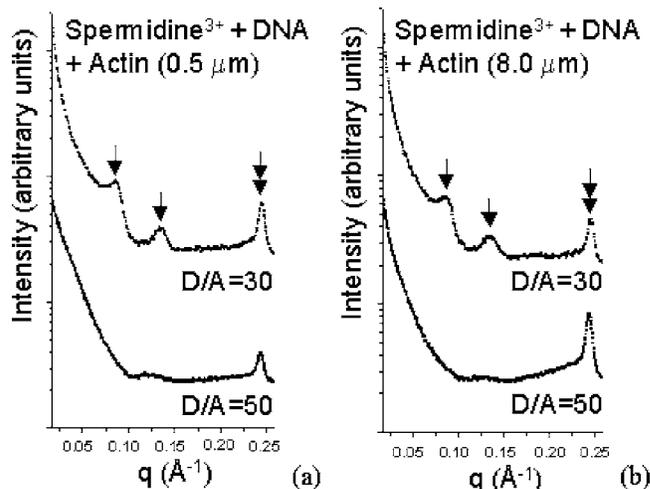
FIG. 6. There are two regimes of behavior for F-actin–DNA mixtures condensed by trivalent salts (spermidine^{3+}). At low D/A ratios, both F-actin and DNA are condensed. At high D/A ratios, only DNA is condensed. (a) Typical SAXS data for samples containing short F-actin (average length 0.5 μm) at 5 mg/ml, λ-DNA at 2.28–3.8 mg/ml, and spermidine^{3+} at 5 mM. Diffraction peaks at 0.086 Å^{-1} and 0.136 Å^{-1} correspond to the bundled phase of F-actin. The peak at 0.245 Å^{-1} corresponds to close-packed DNA. (b) Similar behavior is observed for long F-actin (average length 8 μm) under the same conditions.
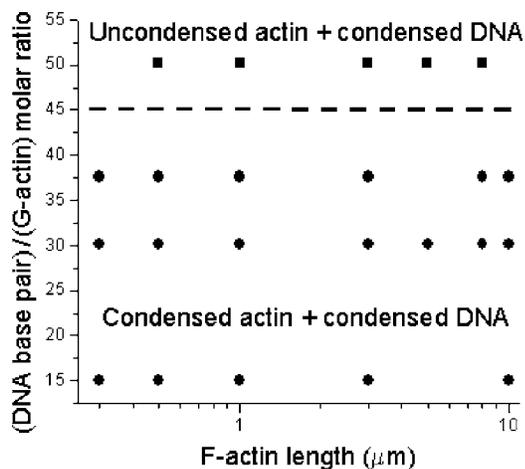
FIG. 7. Phase diagram section for F-actin–DNA–spermidine[3+] system at 5 mM spermidine concentration that is sufficiently high to condense both species in isolation. The F-actin concentration is held constant at 5 mg/ml, while the DNA concentration is varied between 1.14 and 3.8 mg/ml.

sponds to $a = 30$ Å, compared to the hydrated diameter of $D \sim 25$ Å. This agrees well with the measured values from Livolant [84] and Bloomfield [64].

We speculate that it is the surface charge density mismatch between the DNA and F-actin that induces this microphase separation into pure F-actin bundles and pure DNA globules. In this context, it would be interesting to see what happens to mixtures of DNA with polyelectrolytes that have a similar diameter to F-actin but at charge densities that can closely match with DNA.

As the molar ratio between DNA base pairs and G-actin is increased (higher D/A ratio), we observe a decondensation of F-actin, so that only DNA is condensed within the DNA–F-actin mixture. Figure 6(b) shows that as D/A is increased from 30 to 50, the DNA close-packing peak at $q = 0.25$ Å^{-1} is still present while the diffraction peaks that correspond to F-actin packing within the bundles (at $q = 0.086$ Å^{-1} and $q = 0.136$ Å^{-1}) disappear. This is interesting since 5 mM spermidine[3+] is sufficient to condense either component in isolation (which has been independently confirmed by experiment). Moreover, since F-actin has a lower charge density than DNA, it is known to form compact condensed phases more readily: it requires only divalent rather than trivalent ions to condense and exhibits condensation at a lower concentration of trivalent ions. The observed decondensation of F-actin appears to be generic for different F-actin lengths, which we controlled using gelsolin, an actin severing and capping protein. Figure 6 shows that for short and long F-actin rods, similar decondensation occurs as the D/A ratio is increased. A phase diagram representing the phase behavior of F-actin–DNA mixtures in the presence of spermidine for different F-actin lengths is shown in Fig. 7.

Since the minimum concentration of ions required to condense a given polyelectrolyte seems to be an important parameter, it is worthwhile to consider the differences in DNA and F-actin condensation by multivalent ions. In the DNA +multivalent salt system, condensation requires DNA charge neutralization by the ions [85]. In the multicomponent sys-

tem studied here (actin+DNA+spermidine), we indeed see something similar. The condensation threshold exhibits a direct correlation between DNA and spermidine concentrations, as expected from this picture. The same, however, is not true of F-actin [63,71]. In the F-actin+multivalent salt system, the total charge in the multivalent ions at the condensation threshold exceeds the bare charge of F-actin by more than an order of magnitude and the dependence of that threshold on F-actin concentration is relatively weak over a wide range (0.03–10 mg/ml) of global F-actin concentrations. We speculate that this is related to the fact that DNA is a "pure" polyelectrolyte, with only negative charges on its sugar-phosphate backbone, whereas F-actin is a polyelectrolyte with large numbers of negative as well as positive charges that sum to a net negative charge, so it is possible that both counter-ions and co-ions are important.

IV. THEORETICAL DESCRIPTION: FLORY-HUGGINS MODEL

The collective behavior of DNA and F-actin segments in the mixture is determined by a complicated balance between several effects. The presence of multivalent counterions affects the interactions between the similar and the dissimilar species (DNA-DNA, DNA-actin, actin-actin). In particular, the entropy of mixing is expected to play a pivotal role as one expects for any polymer mixture. We present in this section a coarse-grained theoretical description of the DNA–F-actin mixture on length scales beyond the range of the counter-ion-mediated attractions between DNA and actin monomers. To capture the essence of the phase behavior of the DNA–F-actin mixture, we consider a simple phenomenological Flory-Huggins-type theory for a mixture of polymers (DNA), rods (actin), and the solvent. Such a coarse-grained approximation is known to give a qualitative rather than quantitative description of the phase behavior. On this scale, the non-mean-field nature of the system being studied is reflected in the values of the interaction parameters (obtained by integrating out microscopic degrees of freedom) which have attractive contributions which depend on counter-ion density and valence. Let us assume that the polymers are of fixed length N and have a volume fraction of ϕ, the rods are of fixed length L and have a volume fraction of ψ, and naturally, the solvent occupies the rest of the volume with the corresponding fraction being $1 - \phi - \psi$. The free energy associated with this mixture can be written as [86,87]

$$f \equiv \frac{Fa^3}{Vk_\mathrm{B}T} = \frac{\phi}{N}\ln\phi + \frac{\psi}{L}\ln\psi + (1 - \phi - \psi)\ln(1 - \phi - \psi)$$
$$+ \chi_{\mathrm{rp}}\psi\phi + \chi_{\mathrm{rs}}\psi(1 - \phi - \psi) + \chi_{\mathrm{ps}}\phi(1 - \phi - \psi),$$
$$(1)$$

where a is the monomer size, $k_\mathrm{B}T$ is the thermal energy, V is the volume of the sample, and the corresponding χ parameters are defined in a manifest way. In general the condensed (high-density) phase can possess liquid-crystalline order, whose magnitude which can be described by an order parameter.

The above form for the interaction terms (χ parameters) is only justified because the electrostatic correlation-induced attractions are short ranged [88]. To date all the mechanisms proposed for these attractions require going beyond the mean field (Poisson-Boltzmann) so the numerical values of the interaction parameters and their detailed valence dependence must be calculated from a microscopic statistical-mechanical treatment of counter-ions and poly-ions that goes beyond the mean field [89]. Considering the experimental conditions chosen, the χ parameters would have values such that the combinations rod solvent (rs) and polymer solvent (ps) would want to phase separate when alone. We emphasize that the χ parameters are effective interaction coefficients taking account of electrostatic repulsion, counter-ion entropy, and multivalent counter-ion-induced attraction [3–5].

To find the phase behavior of the system, we need to know the structure of the minima of the free-energy function, Eq. (1). For both $\chi_{ps}, \chi_{rs} > 1$ and $\chi_{rp} > |1/N - 1/L|$, one finds that the function has three minima: A, $(\phi_A, \psi_A) = (\phi_0, \psi_0)$; B, $(\phi_B, \psi_B) = (\phi_s, \psi_l)$; and C, $(\phi_C, \psi_C) = (\phi_l, \psi_s)$, where $\psi_0 \simeq e^{-L(\chi_{rs}-1)-1}$, $\phi_0 \simeq e^{-N(\chi_{ps}-1)-1}$, $\phi_s \simeq e^{-N\chi_{rp}-1+N/L}$, $\psi_l \simeq 1 - e^{-(1+\chi_{rs})+1/L}$, $\phi_l \simeq 1 - e^{-(1+\chi_{ps})+1/N}$, and $\psi_s \simeq e^{-L\chi_{rp}-1+L/N}$. Note that the labels l and s correspond to large and small, respectively. In the other parts of the parameter space, the number of minima changes to 2; for $L < N$, $\chi_{rp} < 1/L - 1/N$, A and C will be the minima (B disappears); for $N > L$, $\chi_{rp} < 1/N - 1/L$, there will be A and B left (C disappears); and for $\chi_{ps} < 1$ or $\chi_{rs} < 1$, A vanishes. The minima have clear interpretations: A corresponds to the fully dilute phase, B corresponds to a polymer-poor rod-rich phase, and C corresponds to a polymer-rich rod-poor phase. The "rich" domains would correspond to condensates, while the "poor" domains would just mean the homogeneous phase.

The phase diagram can be determined by using the Maxwell construction. Because the values of ϕ_s, ψ_s, ϕ_0, and ψ_0 are exponentially small, one can assume (to a reasonable approximation) that all those minima are sitting at the boundaries and thus the positions of the common tangent contact points needed for the binodal actually coincide with the minima. In the three-phase coexistence region, we can find the corresponding fractions of each phase in every point of the phase diagram by applying the lever rule to the two fields ϕ and ψ.

Let us assume that we have a fraction x of phase B (corresponding to condensed F-actin), a fraction y of phase C (corresponding to condensed DNA), and a fraction $(1-x-y)$ of phase A. Also assume that we fix (experimentally) the average values for the two fields as $\bar{\phi}$ and $\bar{\psi}$. The lever rule then gives us $\bar{\phi} = x\phi_B + y\phi_C + (1-x-y)\phi_A$ and $\bar{\psi} = x\psi_B + y\psi_C + (1-x-y)\psi_A$, which can be solved to yield the two unknowns x and y as

$$x = \frac{(\bar{\psi} - \psi_0)(\phi_l - \phi_0) - (\bar{\phi} - \phi_0)(\psi_s - \psi_0)}{(\psi_l - \psi_0)(\phi_l - \phi_0) - (\psi_s - \psi_0)(\phi_s - \phi_0)}, \quad (2)$$

$$y = \frac{(\bar{\phi} - \phi_0)(\psi_l - \psi_0) - (\bar{\psi} - \psi_0)(\phi_s - \phi_0)}{(\psi_l - \psi_0)(\phi_l - \phi_0) - (\psi_s - \psi_0)(\phi_s - \phi_0)}. \quad (3)$$
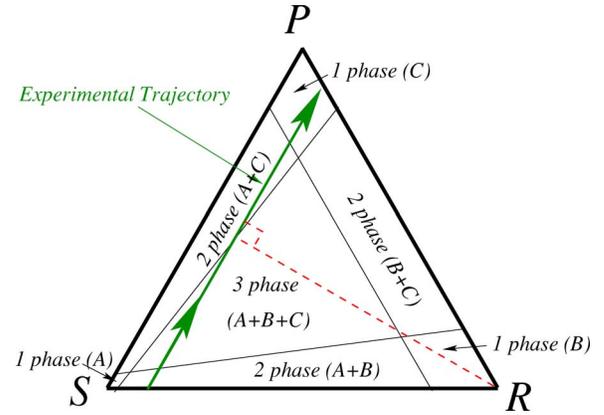
FIG. 8. (Color online) Schematic ternary phase diagram section for the rod-polymer-solvent system for the relevant χ parameters. The line and arrow show the trajectory of the experiments with constant rod (actin) concentration and varying polymer (DNA) concentration.

Let us now go back to the experimentally determined phase diagram of Fig. 7. Putting in numbers we find that the experiment was done at a fixed value of the F-actin volume fraction $\bar{\psi} = 0.005$, while the DNA volume fraction $\bar{\phi}$ was varied from 0.001 to 0.004, which corresponds to the window $0.2 < \bar{\phi}/\bar{\psi} < 0.8$. It appears that the majority of the phase diagram corresponds to the three-phase coexistence region where there are condensed DNA and condensed F-actin phases coexisting with each other as well as the dilute phase. As the ratio between the DNA concentration and the F-actin concentration $\bar{\phi}/\bar{\psi}$ is increased, Eq. (2) shows that the fraction of the F-actin condensate x is decreased. As shown in Fig. 7, the experiment reveals a transition to a state where the F-actin condensate fraction drops to zero at $(\bar{\phi}/\bar{\psi})_T \simeq 0.6$.

A plausible explanation for the observed transition is that it corresponds to crossing the phase boundary between the three-phase and two-phase regions as shown schematically in Fig. 8. This corresponds to the fraction x (of F-Actin) going to zero as $\bar{\phi}/\bar{\psi}$ is increased.

This would yield

$$\left(\frac{\bar{\phi}}{\bar{\psi}}\right)_T = \frac{\phi_0}{\bar{\psi}} + \left(\frac{\phi_l - \phi_0}{\psi_s - \psi_0}\right)\left(1 - \frac{\psi_0}{\bar{\psi}}\right) \quad (4)$$

[see Eq. (2)].

However, in general this yields values of $(\bar{\phi}/\bar{\psi})_T \gg 1$ at the phase transition considerably larger and very different from the observed value of 0.6. Moreover, the value of $(\bar{\phi}/\bar{\psi})_T$ at the phase boundary would depend exponentially on L, while the observed phase boundary is actually independent of L.

Two possible scenarios in which the ratio $(\bar{\phi}/\bar{\psi})_T$ is smaller than 1 can easily be proposed.

(i) If $\bar{\psi}=\psi_0$ and $\psi_0 > \phi_0$, then from Eq. (4) it is clear that $(\bar{\phi}/\bar{\psi})_T < 1$. But this will be true only for a particular actin concentration $\bar{\psi}=\psi_0$.

(ii) A more robust and plausible explanation is that the χ parameters actually depend on the DNA and F-actin concentration [88]. For example, one can imagine that a competition between DNA and F-actin for counter-ion condensation would induce an effective interaction between the F-actin rods that depends on the density of DNA in the solution. The many-body nature of the correlation-induced attraction [3–5] makes it possible that by changing the DNA concentration $\bar{\phi}$ the system crosses over from the three-phase region corresponding to coexistence of condensed F-actin and condensed DNA to the two-phase region that corresponds to uncondensed F-actin and condensed DNA solutions at much *lower* concentrations. This would also be consistent with the observed independence of the phase boundary on the length of the F-actin rods, L.

V. DISCUSSION

A conclusive confirmation of the above picture would require a calculation of the χ parameters based on detailed physical considerations of the correlation-induced attraction in a mixture of F-actin and DNA, which may be a difficult task. Nevertheless, one could use order-of-magnitude estimates to check if the observed onset actually supports this picture. The close-packed DNA globules in the DNA–F-actin mixtures are likely to be fully charge compensated. If we assume that the DNA strands have a much greater affinity for the spermidine trivalent cations, we can estimate the concentration of spermidine^{3+} remaining in solution after the condensation of DNA into globules. For 5 mM spermidine^{3+} and 3.8 mg/ml DNA, the effective spermidine concentration accessible to F-actin is $\sim$1.1 mM. We independently investigated the phase behavior of F-actin alone in the presence of spermidine (Fig. 4) and found that the global concentration at the onset of F-actin condensation is $\sim$1 mM for short ($\sim$3000 Å) filaments and $\sim$1.5 mM for long ($\sim$10 μm) filaments [72]. These "onset" concentrations are close to the estimated concentrations of free spermidine^{3+} using the assumptions stated above. In other words, this comparison suggests that if DNA neutralization is assumed, the effective spermidine^{3+} concentration accessible to F-actin is below the threshold required for F-actin condensation, in agreement with our observed results ("uncondensed actin+condensed DNA" region of the phase diagram in Fig. 7).

In order to test the above proposed model of polyelectrolyte competition for multivalent ions, we have also performed a series of measurements in which the F-actin and DNA concentrations are fixed (actin 5 mg/ml, DNA 3.8 mg/ml) and only the concentration of trivalent ions is changed (Fig. 9). Spermidine concentrations have been varied from the regime where there are insufficient ions to condense both F-actin and DNA (4 mM and 5 mM spermidine^{3+}), to the regime where there are more than enough ions to condense them both (5.5 mM and 6 mM spermidine^{3+}), based on the above charge compensation as-
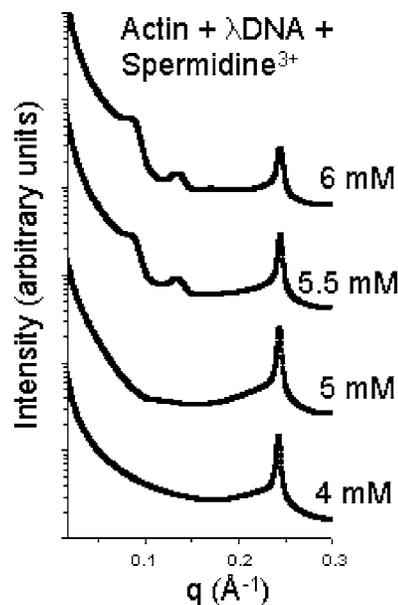
FIG. 9. Increasing amount of trivalent salt in the mixtures with constant F-actin and DNA content leads to the formation of DNA condensates and at high spermidine concentrations to condensation of both DNA and F-actin. Typical SAXS data for samples containing long (10 μm) F-actin at 5 mg/ml, λ-DNA at 3.8 mg/ml, and spermidine^{3+} at 4–6 mM is shown. Diffraction peaks at 0.086 and 0.136 Å^{-1} correspond to the bundled phase of F-actin. The peak at 0.245 Å^{-1} corresponds to close-packed DNA.

sumption. In the former case, we observe DNA condensation only and no F-actin condensation, as evidenced by the lone DNA close-packing correlation peak at $q=0.25$ Å^{-1}. This is consistent with our previous observations described above. However, as the ion concentrations are increased, we begin to see both polyelectrolyte species condense. This can be seen in Fig. 9. As the spermidine concentration is increased, close-packing F-actin correlation peaks (at $q=0.086$ Å^{-1} and $q=0.136$ Å^{-1}) appear in addition to the DNA peaks. Assuming DNA charge neutralization and an experimentally obtained threshold for F-actin condensation alone ($\sim$1.5 mM), both F-actin and DNA are expected to condense above $\sim$5.4 mM spermidine for long 10-μm actin filaments (for short filaments the predicted threshold is lower, $\sim$5 mM). This is quite close to the experimentally observed values: DNA and F-actin begin to cocondense between 5 mM and 5.5 mM. We note that the effect of polydispersity in the length of the F-actin rods should also be taken into account for a full quantitative analysis of the experimental results. Nevertheless, these observations are consistent with our model, since an increase in the ion concentration leads to decreased competition.

The phase behavior of these mixed polyelectrolyte systems with multivalent ions may be important in a number of contexts outside polyelectrolyte physics. For example, antibiotics such as the aminoglycosides, which are multivalent cationic sugars, are used to treat long-term infections in cystic fibrosis (CF) patients. However, the accumulation of anionic DNA and F-actin released during inflammation in CF airways is thought to contribute to the adventitious binding

and inactivation of antibiotics and endogenous antibacterial peptides. An understanding of the underlying polyelectrolyte effects may contribute to new therapeutic strategies.

In summary, we have examined the condensation behavior of F-actin–DNA mixtures in the presence of ions of different valences and find that these binary anionic polyelectrolyte mixtures exhibit a rich range of behavior. In these mixtures, the existence of one polyelectrolyte component can modulate the condensation behavior of the other polyelectrolyte component. In the present system under investigation, the existence of DNA can lead to the decondensation of F-actin in F-actin–DNA mixtures. These observations may have important implications in the rational control of interactions in complex fluid mixtures.

[1] J. Israelachvili, *Intermolecular and Surface Forces* (Academic Press, London, 1992).

[2] A. Y. Grosberg and A. R. Khokhlov, Adv. Polym. Sci. **41**, 53 (1981).

[3] Y. Levin, Rep. Prog. Phys. **65**, 1577 (2002).

[4] W. M. Gelbart, R. F. Bruinsma, P. A. Pincus, and V. A. Parsegian, Phys. Today **53** (9), 38 (2000).

[5] C. Holm, P. Kékicheff, and R. Podgornik, *Electrostatic Effects in Soft Matter and Biophysics* (Kluwer Academic, Dordrecht, 2001).

[6] M. LeBret and B. H. Zimm, Biopolymers **23**, 287 (1984).

[7] L. N. Guldbrand, L. Nilsson, and L. Nordenskiöld, J. Chem. Phys. **85**, 6686 (1986).

[8] C. F. Anderson and M. T. Record, Jr., Annu. Rev. Biophys. Biophys. Chem. **19**, 423 (1990).

[9] G. Lamm, L. Wong, and G. R. Pack, Biopolymers **34**, 227 (1994).

[10] L. G. Nilsson, L. Guldbrand, and L. Nordenskiöld, Comp. Biochem. Physiol., Part A: Mol. Integr. Physiol. **72**, 177 (1991).

[11] J. G. Kirkwood and J. B. Shumaker, Proc. Natl. Acad. Sci. U.S.A. **38**, 863 (1952).

[12] F. Oosawa, Biopolymers **6**, 1688 (1968).

[13] F. Oosawa, *Polyelectrolytes* (Dekker, New York, 1971).

[14] J. Ray and G. S. Manning, Langmuir **10**, 2450 (1994).

[15] A. P. Lyubartsev and L. Nordenskiöld, J. Phys. Chem. **99**, 10373 (1995).

[16] A. P. Lyubartsev and L. Nordenskiöld, J. Phys. Chem. B **101**, 4335 (1997).

[17] I. Rouzina and V. A. Bloomfield, J. Phys. Chem. **100**, 9977 (1996).

[18] I. Rouzina and V. A. Bloomfield, Biophys. Chem. **64**, 139 (1997).

[19] N. Grønbech-Jensen, R. J. Mashl, R. F. Bruinsma, and W. M. Gelbart, Phys. Rev. Lett. **78**, 2477 (1997).

[20] B.-Y. Ha and A. J. Liu, Phys. Rev. Lett. **79**, 1289 (1997).

[21] B.-Y. Ha and A. J. Liu, Phys. Rev. Lett. **81**, 1011 (1998).

[22] R. M. Nyquist, B.-Y. Ha, and A. J. Liu, Macromolecules **32**, 3481 (1999).

[23] R. Podgornik and V. A. Parsegian, Phys. Rev. Lett. **80**, 1560 (1998).

[24] F. J. Solis and M. Olvera de la Cruz, Phys. Rev. E **60**, 4496 (1999).

[25] A. P. Lyubartsev, J. X. Tang, P. A. Janmey, and L. Nordenskiöld, Phys. Rev. Lett. **81**, 5465 (1998).

[26] B. I. Shklovskii, Phys. Rev. Lett. **82**, 3268 (1999).

[27] B. I. Shklovskii, Phys. Rev. E **60**, 5802 (1999).

[28] V. I. Perel and B. I. Shklovskii, Physica A **274**, 446 (1999).

[29] T. T. Nguyen, A. Y. Grosberg, and B. I. Shklovskii, Phys. Rev. Lett. **85**, 1568 (2000).

[30] T. T. Nguyen, A. Y. Grosberg, and B. I. Shklovskii, J. Chem. Phys. **113**, 1110 (2000).

[31] T. T. Nguyen, I. Rouzina, and B. I. Shklovskii, J. Chem. Phys. **112**, 2562 (2000).

[32] T. T. Nguyen and B. I. Shklovskii, Phys. Rev. E **64**, 041407 (2000).

[33] T. T. Nguyen and B. I. Shklovskii, Physica A **293**, 324 (2001).

[34] A. A. Kornyshev and S. Leikin, Phys. Rev. Lett. **82**, 4138 (1999).

[35] T. G. Dewey, Biopolymers **29**, 1793 (1990).

[36] E. Rajasekaran and B. Jayaram, Biopolymers **34**, 443 (1994).

[37] K. Sharp, Biopolymers **36**, 227 (1995).

[38] K. A. Sharp, R. A. Friedman, V. Misra, J. Hecht, and B. Honig, Biopolymers **36**, 245 (1995).

[39] M. J. Stevens, Phys. Rev. Lett. **82**, 101 (1999).

[40] M. C. Barbosa, M. Deserno, and C. A. Holm, Europhys. Lett. **52**, 80 (2000).

[41] J. J. Arenzon, J. F. Stilck, and Y. Levin, Eur. Phys. J. B **12**, 79 (1999).

[42] J. J. Arenzon, Y. Levin, and J. F. Stilck, Physica A **283**, 1 (2000).

[43] A. Diehl, H. A. Carmona, and Y. Levin, Phys. Rev. E **64**, 011804 (2001).

[44] M. Deserno, A. Arnold, and C. Holm, Macromolecules **36**, 249 (2003).

[45] H. Schiessel and P. Pincus, Macromolecules **31**, 7953 (1998).

[46] P. L. Hansen, D. Svensek, V. A. Parsegian, and R. Podgornik, Phys. Rev. E **60**, 1956 (1999).

[47] R. Podgornik, P. L. Hansen, and V. A. Parsegian, J. Chem. Phys. **113**, 9343 (2000).

[48] P. L. Hansen, R. Podgornik, and V. A. Parsegian, Phys. Rev. E **64**, 021907 (2001).

[49] R. Golestanian and T. B. Liverpool, Phys. Rev. E **66**, 051802 (2002).

[50] R. Golestanian, M. Kardar, and T. B. Liverpool, Phys. Rev. Lett. **82**, 4456 (1999).

[51] I. Borukhov, K. C. Lee, R. F. Bruinsma, W. M. Gelbart, A. J.

Liu, and M. J. Stevens, J. Chem. Phys. **117**, 462 (2002).

[52] I. Borukhov, R. F. Bruinsma, W. M. Gelbart, and A. J. Liu, Phys. Rev. Lett. **86**, 2182 (2001).

[53] T. E. Angelini, H. Liang, W. Wriggers, and G. C. L. Wong, Proc. Natl. Acad. Sci. U.S.A. **100**, 8634 (2003).

[54] A. Y. Grosberg, T. T. Nguyen, and B. I. Shklovskii, Rev. Mod. Phys. **74**, 329 (2002).

[55] G. S. Manning, Q. Rev. Biophys. **2**, 179 (1978).

[56] R. W. Wilson and V. A. Bloomfield, Biochemistry **18**, 2192 (1979).

[57] V. A. Bloomfield, R. W. Wilson, and D. C. Rau, Biophys. Chem. **11**, 339 (1980).

[58] J. Widom and R. L. Baldwin, J. Mol. Biol. **144**, 431 (1980).

[59] I. Baeza, P. Gariglio, L. M. Rangel, P. Chavez, L. Cervantes, C. Arguello, C. Wong, and C. Montanez, Biochemistry **26**, 6387 (1987).

[60] P. G. Arscott, A.-Z. Li, and V. A. Bloomfield, Biochemistry **30**, 619 (1990).

[61] V. A. Bloomfield, Biopolymers **31**, 1471 (1991).

[62] C. Ma and V. A. Bloomfield, Biophys. J. **19**, 234 (1994).

[63] V. A. Bloomfield, Curr. Opin. Struct. Biol. **6**, 334 (1996).

[64] V. A. Bloomfield, Biopolymers **44**, 269 (1997).

[65] H. Deng, V. A. Bloomfield, J. M. Benevides, and G. J. Thomas, Nucleic Acids Res. **28**, 3379 (2000).

[66] H. Deng and V. A. Bloomfield, Biophys. J. **77**, 1556 (1999).

[67] D. C. Rau and V. A. Parsegian, Biophys. J. **61**, 246 (1992).

[68] R. Podgornik, D. C. Rau, and V. A. Parsegian, Biophys. J. **66**, 962 (1994).

[69] R. Marquet and C. Houssier, J. Biomol. Struct. Dyn. **9**, 159 (1991).

[70] J. X. Tang and P. A. Janmey, J. Biol. Chem. **271**, 8556 (1996).

[71] J. X. Tang, S. Wong, P. T. Tran, and P. A. Janmey, Ber. Bunsenges. Phys. Chem. **100**, 796 (1996).

[72] G. C. L. Wong, A. Lin, J. X. Tang, Y. Li, P. A. Janmey, and C. R. Safinya, Phys. Rev. Lett. **91**, 018103 (2003).

[73] I. Borukhov and R. F. Bruinsma, Phys. Rev. Lett. **87**, 158101 (2001).

[74] J. C. Butler, T. Angelini, J. X. Tang, and G. C. L. Wong, Phys. Rev. Lett. **91**, 028301 (2003).

[75] T. Iwataki, S. Kidoaki, T. Sakaue, K. Yoshikawa, and S. S. Abramchuk, J. Chem. Phys. **120**, 4004 (2004).

[76] H. Kuramochi and Y. Yonezawa, J. Biosci. Bioeng. **92**, 183 (2001).

[77] J. Viamontes and J. X. Tang, Phys. Rev. E **67**, 040701(R) (2003).

[78] J. Viamontes and J. X. Tang, e-print cond-mat/0506813.

[79] Z. Y. Chen, Macromolecules **26**, 3419 (1993).

[80] O. V. Zribi, J. C. Butler, R. Golestanian, T. Liverpool, and G. C. L. Wong (unpublished).

[81] M. L. Henle and P. A. Pincus, e-print cond-mat/0407645.

[82] B.-Y. Ha and A. J. Liu, Europhys. Lett. **46**, 624 (1999).

[83] C. Huang and M. O. de la Cruz, Macromolecules **35**, 976 (2002).

[84] F. Livolant, Prog. Polym. Sci. **21**, 1115 (1996).

[85] E. Raspaud, M. O. de la Cruz, J.-L. Sikorav, and F. Livolant, Biophys. J. **74**, 381 (1998).

[86] M. Rubinstein and R. Colby, *Polymer Physics* (Oxford University Press, New York, 2003).

[87] K. Bergfeldt, L. Piculell, and P. Linse, J. Phys. Chem. **100**, 3680 (1996).

[88] A number of different mechanisms have been proposed for correlations leading to the attractive interactions observed in charged systems summarized in Refs. [3–5]. The shortest scale for the range of attractive interactions is a molecular one while the longest scale is given by half the Debye screening length of the solution. For our analysis, it is sufficient that the range of the attractive interaction is finite (i.e., much less than the system size).

[89] T. Liverpool and K. Müller-Nedebock (unpublished).